



REGULAR PAPER

Re-entry vehicle performance analysis under the control of lateral jet

S.P. Sanaka¹, R.K. Sharma², G.V. Ramana Murty³ and K. Durga Rao⁴

¹Department of Mechanical Engineering, V R Siddhartha Engineering College, Vijayawada, India, ²DRDO, Hyderabad, India,

³Department of Mechanical Engineering, Vasavi College of Engineering, Hyderabad, India and ⁴Department of Mechanical Engineering, University College of Engineering, Adikavi Nannaya University, Rajahmundry, India

Corresponding author: S. P. Sanaka; Email: drssp1974@gmail.com

Received: 18 March 2023; **Revised:** 23 July 2023; **Accepted:** 26 July 2023

Keywords: aerodynamics; CFD; hypersonic flow; RCS; jet interaction

Abstract

Lateral jets are used to control the missiles and re-entry vehicles at high altitudes. The objective of the research paper is to investigate the effect of lateral jet interaction with the external flow on a blunted nose cone re-entry vehicle configuration and its flight speed. Structured mesh is used for the simulations, and the computational analysis is carried out by Ansys Fluent solver. The simulation results are validated, and the same methodology used for the parametric analysis. Simulations have been carried out at an external flow Mach number 6, 8.1, 12 and 16 at five degree angle-of-attack for jet-off and jet-on conditions. At 8.1 Mach number, the normal force coefficient is decreased by 45.6% due to jet interaction. The lateral jet interaction effectively reduces the nose down pitching moment. At 8.1 Mach number, the pitching moment coefficient was reduced by 48% with the jet-on condition compared to the jet-off condition.

Nomenclature

C_A	axial force coefficient
C_m	moment coefficient
C_N	normal force coefficient
C_p	pressure coefficient
d	reference diameter
M_∞	mach number
p	static pressure
T	temperature
p_∞	free stream pressure
X_{cp}/d	centre of pressure (C_m/C_N)
α	angle-of-attack
u_τ	friction velocity (m/s)
y	distance from the surface in the boundary layer (m)
ν	kinematic molecular viscosity (m^2/s)

1.0 Introduction

The lateral jet control system is a subsystem of a spacecraft/re-entry vehicle/missile. Its purpose is to provide attitude control and steering. The lateral jet control system provides necessary control for the re-entry vehicle to follow the pre-planned trajectory. Lateral jets are used to control the flight vehicle at

high altitudes during the ascent and descent phases, especially where the dynamic pressure is low. The lateral jet is issued perpendicular to the surface of the vehicle and interacts with the external flow, causing pressure changes along the surface from the nose to the base in the direction of the vehicle's axis. The magnitude of the aerodynamic forces is influenced by the interaction with the lateral jet. Experiments are carried out on a blunted cone at a free stream Mach number of 8.1 using the shock tunnel at Nagoya University, Japan [1] and reported that the jet interaction region extends toward the upstream of the jet nozzle as α increases from 0 to 40°. Kurita et al. [2] investigated the side jet interaction with the Mach 3 external flow on the blunted cone at $\alpha = 0$ to 40° at an interval of 5 degrees [3]. The side jet interaction with free stream flow at $M_\infty = 2.2$ studied on a typical missile configuration along with control surfaces at low altitude [4] and noticed that amplification has opposing effect at $\alpha = -15^\circ$ angle-of-attack as compared to the zero and 15 degrees. Gnemmi and Seiler [5] studied the lateral jet interaction phenomena with 4.5 Mach external flow at 7km altitude. Experiments are carried out on missile configuration in the Institute of Saint Louis (ISL) shock tube in France and predicted the force and moments amplification factors. Erinc Erdem and Konstantinos Kontis [6] experimentally investigated the interaction of jet issued from flat plate with $M_\infty = 5$ free stream flow over a plate and captured the jet interaction flow field. Srivastava et al. [7] utilised computational fluid dynamics (CFD) for analysing missile configurations with reaction control jets. The results were validated and summarised, demonstrating that CFD has enormous potential as a tool for studying lateral jet interaction studies. Hsieh [8] investigated the jet interaction studies on axisymmetric configuration at various angle-of-attack, $M_\infty = 9.7$ and summarised that the recirculation region in the upstream region of the jet is strong at positive incidence and weak at negative incidence. Gimelshein et al. [9] studied the lateral jet influence at altitudes of 80, 90 and 100km. The investigation employed free stream velocities of 2, 3 and 4km/s, while the jet was injected with a velocity of 2,540m/s. The study elucidated the impact of height, α (angle-of-attack) and rocket velocity on the induced flow structure. The influence of the jet issued into the Mach 8.1 free stream flow on blunt body was simulated numerically by Nakamura Tetsuya et al. [10] studied and summarised that jet interaction augments the thrust force generated by the lateral jet. The analysis was carried out at 0°, 20°, 40° angle-of-attack. Valerio Viti and Joseph Schetz [11] have used Spalart Allmaras and K-omega turbulence models to study the jet interaction with 4 Mach external flow with and without jet and concluded that the lateral jet interaction increased the jet reaction force. Gnemmi et al. [12] investigated the interaction between the side jet delivering from axisymmetric body and the free stream flow with $M_\infty = 3$ using CFX-TASCflow software. The aerodynamic force and moment coefficients have been compared with and without jet. Gnemmi et al. [13] have validated the computational methodology adopted for the jet interaction study on generic missile configuration. Computations are carried out at $M_\infty = 2.8$, $\alpha = -5, 0$ and 10°. The flow field structures such as flow separation and Mach disk are captured. Aswin and Debasis [14] numerically studied the lateral jet communication with the cross flow. Flight vehicle selected was a missile configuration. Computations are carried out with multi-jets located at various locations on missile to notice the result of jet position. The zone of interaction between cross flow and the jets was augmented with the three jets than two jets. Imran Rasheed et al. [15] studied the interaction between a sonic jet issued from a flat plate and free stream flow at $M_\infty = 1.6$ and identified the flow field associated with shocks and recirculation zones. The efficiency of positioned synthetic jet and a row of four circular synthetic jets was compared [16] and the study demonstrated that the efficiency of slotted synthetic jets is better than that of a row of circular jets for improving aerodynamic performance. The control forces generated by the side jet during the flight were computed [17]. Choi et al. [18] carried out a numerical simulation on a blunt cone cylinder body shaped interceptor at a flight speed of Mach 6. They predicted the changes in aerodynamic coefficients by varying the angle-of-attack from -20 to 20 degrees. The sonic jet interaction flow field topology was studied [19] at an external flow of Mach 9.84, altitudes of 50, 60 and 70km using Open FOAM software and concluded that the induced sonic jet interaction flow topology around the generic missile changed with altitude. Two modeling approaches are used to study the interaction of side jet issued from a missile with continuous-type side-jet systems [20]. One method was the CFD-based modeling and the other was the surrogate modeling. Surrogate modeling method will play an important role in the jet-interaction analysis. Warrick A Miller et al. [21]

investigated the computational flow structure induced due to the interaction of sonic reaction control jet issued from a flat plate and Mach 5 cross flow. Chen [22] simulated the lateral jet interaction with transonic flow on 45mm base diameter of ogive cylinder configuration and noticed that the jet amplification factor decreases with $\alpha = 0-10$ degree. Jiawei Zhang et al. [23] demonstrated that the introduction of the reaction control jet among the canards and the fins can efficiently control roll coupling. Dong Haibo et al. [24] studied the side jet interaction flow field in supersonic flow and the flow field structure and pressure distribution obtained from numerical solution was validated on cone cylinder flare model in Mach 3 supersonic cross flow. Dong et al. [25] numerically studied the drag reduction on a hemi spherical nose with a spike having cylindrical body with the use of lateral jet. The effect of location of jet and the number jet have been studied and concluded that the drag was reduced by 38.81% with the use of dual jets at different locations. Majie Zhao et al. [26] investigated the jet interaction flow field structure and mixing features of a single and two gas jets injected into high-speed cross flow. They observed that the penetration and mixing characteristics are superior with two jets. Raj Kiran Grandhi and Arnab Roy [27] studied the influence of curvature of flight vehicle and height on the effectiveness of the lateral jet interaction. The study reported that the jet thrust decreased and caused a pitch down moment of the vehicle. Jinping LI [28] studied the lateral jet interaction with cross flow using Bayesian method and wall pressure was predicted by the Spalart-Allmaras turbulence model and noticed that percentage of error was reduced from 14.99% to 2.95%. Malsur Dharavath et al. [29] investigated the lateral jet interaction with supersonic cross flow using Ansys CFX commercial software and summarised that separation in front of the lateral jet amplified with increase in jet pressure ratio and the slot width enhances the interaction. Several studies are available on jet interaction flow field analysis, prediction of aerodynamic characteristics of missile configurations during the interaction. Literature pertaining to the computational studies on the transverse jet interaction with the external flow on re-entry vehicle is limited. The computational data pertaining to the pressure and aerodynamic coefficients distributions along the axial and radial direction available is low. Jet interaction also depends on the external flow Mach number. Therefore, the jet interaction data was compared with jet-off condition to understand the influence of jet interaction in this paper and also investigated the influence of flight speed on jet interaction.

2.0 Re-entry vehicle shape considered for the investigation

The model selected for the investigation is a blunt cone representing a typical re-entry vehicle. It consists of a spherical nose followed by the cone with 10.3° semi apex angles and the nose bluntness ratio is 52.3%. The base diameter of the vehicle is 76.5mm. The location of the jet is 0.33 times of diameter from the base of vehicle and the jet diameter is 2mm. The length of the flight vehicle considered is 1.568d. The isometric view of the chosen re-entry model is shown in Fig. 1. This model was chosen because there is available experimental data for validation purposes. The position of centre of gravity, centre of pressure and the sign convention followed for aerodynamic forces and pitching moments is depicted in Fig. 2. Fineness ratio is the ratio of the re-entry configuration axial length to its base diameter. Fineness ratio of the re-entry configuration is 1.568.

3.0 Grid used for analysis

Inflow domain is considered around the body is in parabolic shape and the outflow domain is considered in the plane of base to control the solution and reduce the computational effort. The parabolic fluid domain considered around the flight vehicle configuration is discretised and the structured mesh distribution in the top and side views is depicted in Fig. 3. The mesh shown reveals details such as the parabolic shape of the fluid domain, the locations of fine mesh and variations in cell height. Number of hexahedral elements used for the simulation is 0.225m. Very fine grid is used around the jet. The first cell height defined is 0.0036mm and it was selected based on the operating conditions. All mesh stretching was kept below a ratio of 1.1. Fine mesh is used around the lateral jet to capture the jet interaction

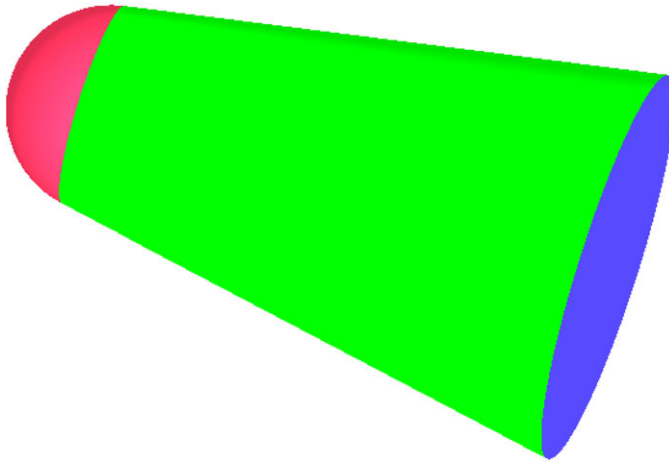


Figure 1. Isometric view of the reentry vehicle.

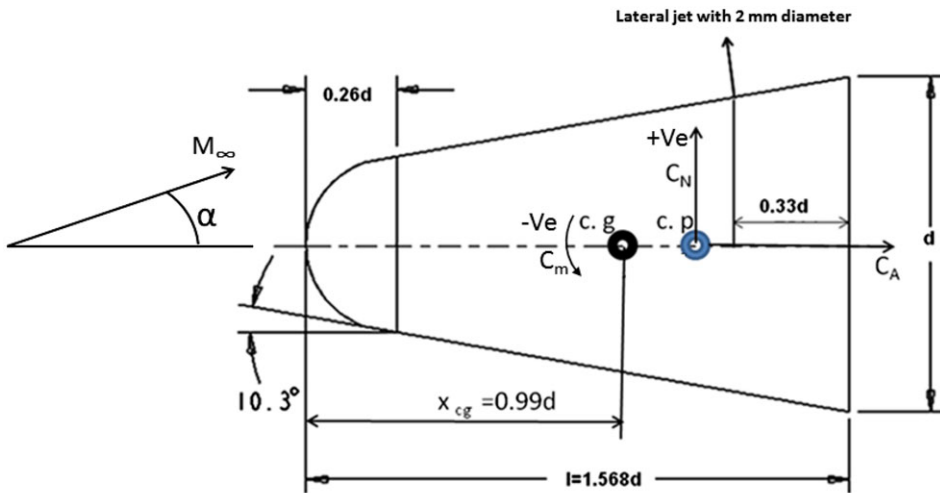


Figure 2. Schematic view of model with sign convention used for force and moment.

influence. The adequacy of the normal spacing was assessed by calculating the y^+ for the cells on the blunt cone surface ahead of the separation region. All the cells adjacent to the solid surface were below y^+ of 1.0. This spacing close to the wall is a widely accepted value for accurate predictions using the $k-\omega$ SST Turbulent model, in wall bounded turbulent flows. In general, the height of the first cell was calculated from Equation (1).

$$y^+ = \frac{u_\tau * y}{\nu} \tag{1}$$

4.0 Computational methodology

The Ansys Fluent solver is used for the simulations. The computations have been performed using an implicit fluid flow solver. Steady state, three dimensional, compressible fluid flow simulations are carried out by considering air as ideal gas. The operating pressure used is 0 and $k-\omega$ Shear Stress Transport (SST) turbulence model is used for the simulations. The boundary conditions used for the simulation

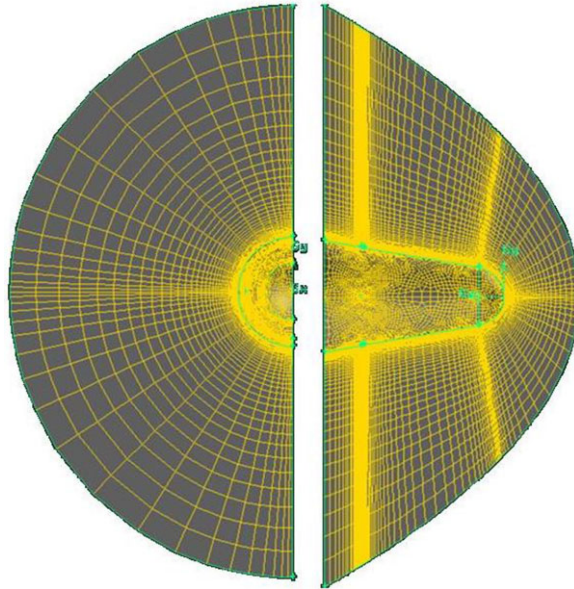


Figure 3. Structured grids in the fluid domain shown in the top and side views.

include the far field condition at the fluid domain inlet, an outflow condition at the outlet, and a mass flow inlet condition to define the jet conditions. External flow direction is defined by using the X and Y component of velocity. The Mach number is varied from 6 to 16 at $\alpha = 5^\circ$. The lateral jet is issued with the mass flow rate of 0.068 kg/s and the nozzle exit pressure defined is 0.64 MPa. Nozzle pressure ratio used is 1.16×10^3 . Courant number used is less than five to control the solution. It is one of the important parameter to resolve convergence issues arise during the solution. Turbulent viscosity used is 1% of the upstream flow at inlet boundary condition. The static pressure and static temperature defined for the external flow simulation is $P_\infty = 550$ Pa and 267.3 K. The pressure and temperature values are considered at an altitude of 35 km.

5.0 Results and discussion

5.1 Validation studies

Experimental data Kurita et al. [1] is available on blunt cone body at $\alpha = 0^\circ$ with jet-on at 8.1 Mach number. These experiments were conducted at Nagoya university shock tube, Japan. The circular jet is injected normal to the flight vehicle surface on leeward side. The operating conditions used for the simulation for validation are the same as those used in the experiments carried out. The computed surface pressure variation along the axis on the leeward side of the vehicle has been compared with the jet-on condition at $\alpha = 0^\circ$ with $M_\infty = 8.1$ is shown in Fig. 4. The jet is located is at a distance of $x/L = 0$. The pressure is increased in front of the jet due to the presence of lateral jet. The computational results are very close to the test data for jet-on condition.

The Mach contours at $\alpha = 0^\circ$, $M_\infty = 8.1$ is compared with the schlieren image in Fig. 5. However, small a discrepancy in the flow field is observed.

5.2 Effect of lateral jet interaction on axial and circumferential pressure distribution

Axial distribution of computed pressure coefficient with jet-off and jet-on was plotted in Fig. 6 at $\alpha = 5^\circ$ to analyse the spatial interaction of the lateral jet with the external flow. The variation of pressure

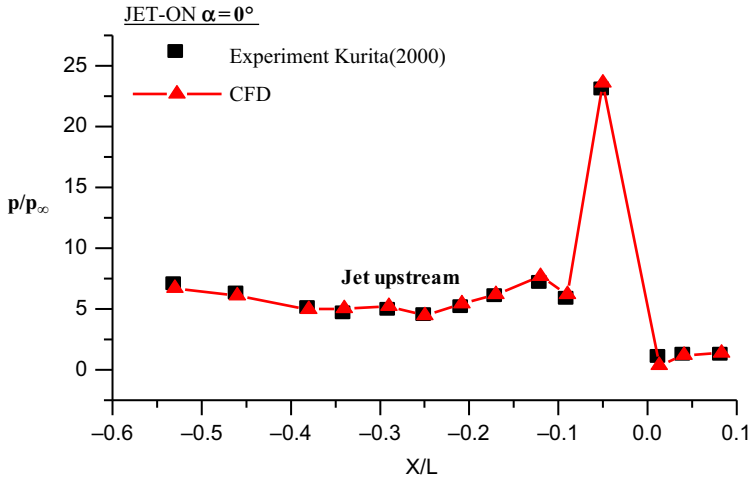


Figure 4. Comparison of CFD surface pressure with experimental data for jet-on at $\alpha = 0^\circ$.

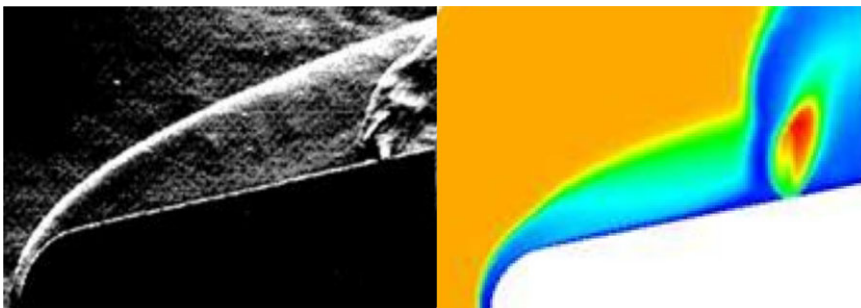


Figure 5. Mach contours comparison with the schlieren image at $\alpha=5^\circ$, $M_\infty = 8.1$.

distribution on the vehicle leeward surface along the longitudinal axis from nose to base is smooth for jet-off condition. The pressure coefficient is not varying abruptly on the leeward surface in pitch plane near the location of the jet. The stagnation pressure coefficient at the nose of the vehicle is 1.827. A relatively small stagnation region formed ahead of the jet for jet-on condition and local pressure is increased above jet-off values. In the induced jet interaction region, upstream of the jet, the surface pressure is raised slightly due to jet separation shock and it is so largely due to the jet bow shock in the upstream of the jet. The computed circumferential pressure distribution for jet-off and jet-on conditions is shown in Fig. 7 at $\alpha = 5^\circ$, $M_\infty = 8.1$. The interaction of the lateral jet with the external flow in the circumferential direction is represented by the interaction region marked with shaded lines. The jet interaction region is in between $\varphi = 275^\circ$ to 85° . Jet pressure ratio (JPR) is the ratio of the jet static pressure to free stream static pressure.

5.3 Effect of lateral jet interaction on aerodynamic coefficients

The normal force coefficient distribution along the longitudinal direction with jet-off and jet-on has been plotted in Fig. 8. The variation of normal force coefficient with jet-off and jet-on till ahead of the jet is almost same. For jet-on condition, it was observed that the magnitude of normal force coefficient starts decreasing from $x/d = 1.03$ to $x/d = 1.236$ (location of jet). This reduction in normal force is due to the positive pressure acting on vehicle downwards ahead of the jet. Downstream of the jet, the pressure

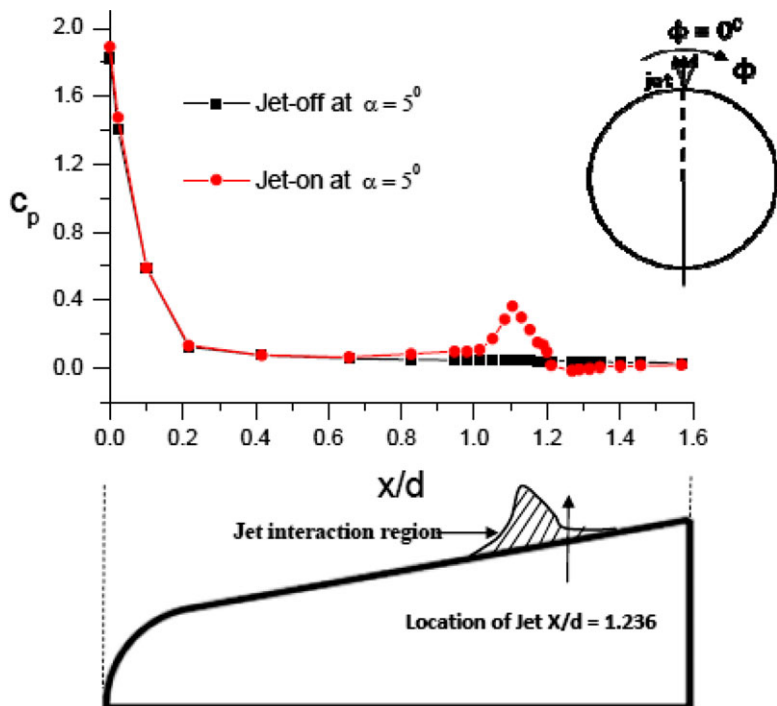


Figure 6. Leeward pressure distribution with jet-off and jet-on along the axial direction at $\alpha = 5^\circ$, $M_\infty = 8.1$, $\Phi = 0^\circ$.

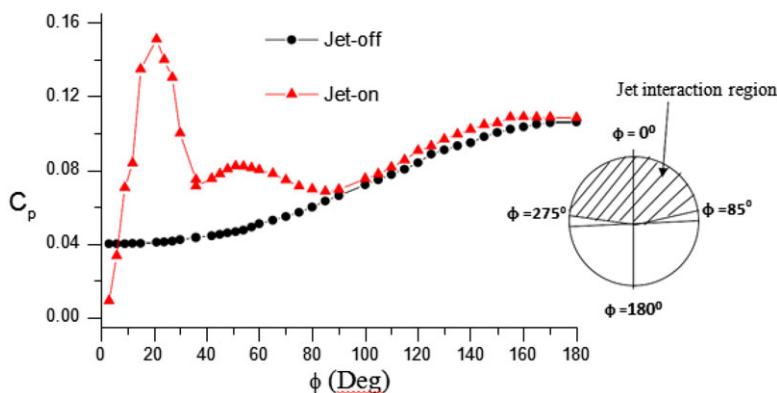


Figure 7. Pressure coefficient in a plane ($x/d = 1.236$) with jet-off and jet-on at $\alpha = 5^\circ$, $M_\infty = 8.1$, $JPR = 1,100$, mass flow rate = 0.068kg/s .

decreases due to the effect of entrainment. Therefore, the normal force coefficient starts recovering from $x/d = 1.236$ (Location of jet) to $x/d = 1.56$ (base of the vehicle). After the jet, the normal force coefficient is recovered by 13.12%. Therefore, the loss of normal force coefficient for complete configuration with jet-on reduced by 45.6% compared with jet-off. The pitching moment coefficient and centre of pressure distribution with jet-off and jet-on along the longitudinal direction has been plotted in Figs 9 and 10. The pitching moment coefficient and centre of pressure with jet-off and jet-on are same till $x/d = 0.91$. Pitching moment coefficient decreased from $x/d = 0.91$ to $x/d = 1.236$. The moment coefficient was recovered significantly in the downstream of the jet due to the low pressure region behind the jet.

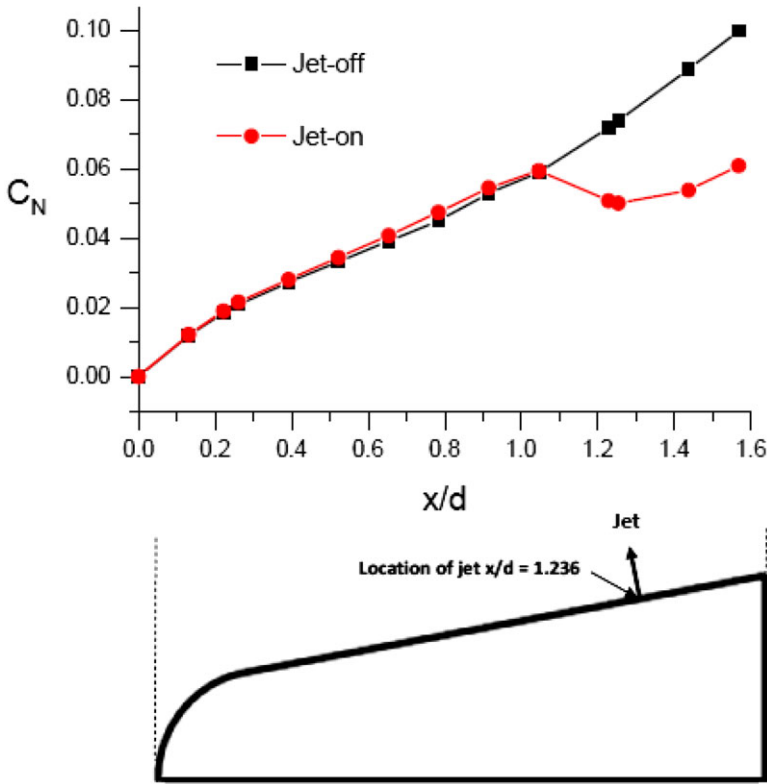


Figure 8. C_N distribution along the axial length at $\Phi = 0^\circ$ with jet-off and jet-on at $\alpha = 5^\circ$, $M_\infty = 8.1$, $JPR = 1,100$, leeward jet mass flow rate = 0.068kg/s , altitude = 35km .

The overall centre of pressure shifts forward by $0.06d$, indicating the loss of stability with jet-on condition compared with jet-off condition. This reduction is more predominant. Designer should consider adequate margin in the stability of the re-entry vehicle since it is necessary be statically stable during re-entry.

5.4 Effect of Mach number on jet interaction flow field

Numerical simulations have been carried out for jet-on condition on the configuration selected at different Mach numbers ($M_\infty = 6, 8, 12$ and 16). The operating conditions used for the simulations are given in Table 1.

5.4.1 The influence of external flow on jet interaction flow field

The flow fields are analysed and demonstrated by the contours of Mach number in pitch plane. The dominant features of the jet interaction between the lateral jet and the external flow are illustrated in Fig. 11. A detailed flow field topology in the pitch plane near the lateral jet region is indicated. The jet creates the obstacle for the external flow which produces bow shock. The lateral jet exhausting at a right angle into external flow produces an inclined barrel shock, since the jet is being under expanded, terminates in a Mach disk. The barrel shock acts as a blunt body obstruction to the incoming flow thus forming a detached bow shock. The jet plume is turned in the direction of the external flow and the Mach disk structure, which commonly encountered in highly under expanded axisymmetric jet exhausting into still air is observed. A fully developed turbulent boundary layer is present at the upstream inlet

Table 1. Flight and jet conditions used for analysis

S No	Mach number	Jet pressure ratio	Angle-of-attack (degrees)	Altitude (km)	Jet mass flow rate (kg/s)	Location of the jet
1	6	1,100	5	35	0.068	leeward
2	8.1	1,100	5	35	0.068	leeward
3	12	1,100	5	35	0.068	leeward
4	16	1,100	5	35	0.068	leeward

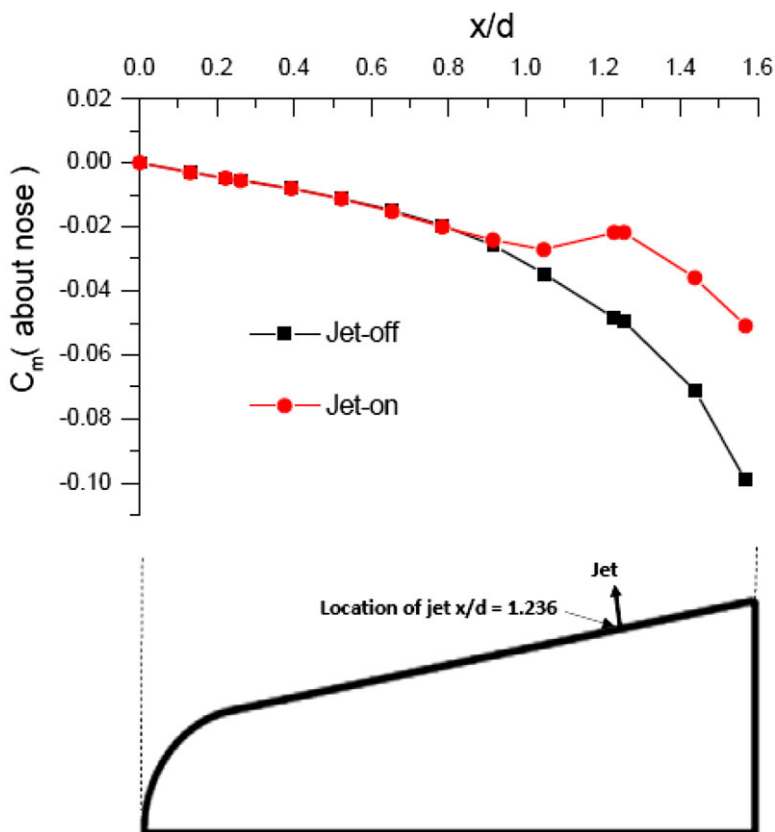


Figure 9. C_m distribution along the axial length at $\Phi = 0^\circ$ with jet-off and jet-on at $\alpha = 5^\circ$, $M_\infty = 8.1$, $JPR = 1,100$, leeward jet mass flow rate = 0.068kg/s, altitude = 35km.

and as it approaches the adverse pressure gradient created by the bow shock wave, it separates from the tunnel flow. Looking at the interior volume of the barrel shock, a large expansion fan is present with its boundaries defined by a recompression shock that ends with a Mach disk. The flow field features of the jet interaction observed in this research is consistent with the results [11–13].

Mach contours at different flight speed are shown in Fig. 12. These Mach contours indicate that, stronger shocks and expansions are observed at higher Mach number flow. The increased Mach number implies a stronger interaction between the jet and the approaching flow, which will tend to increase the extent of separation in the upstream of the jet. At low Mach number, the reaction control jet flow expands straight and jet bow shock is in front of jet location and it bends back at higher Mach number. A small

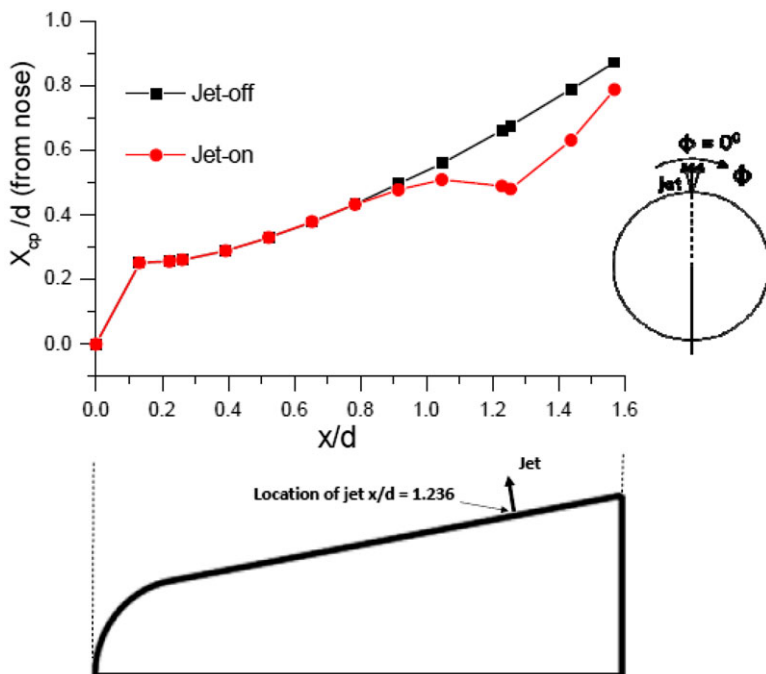


Figure 10. Centre of pressure plotted at $\Phi = 0^\circ$ with jet-off and jet-on at $\alpha = 5^\circ$, $M_\infty = 8.1$, $JPR = 1,100$, leeward jet mass flow rate = 0.068kg/s , altitude = 35km .

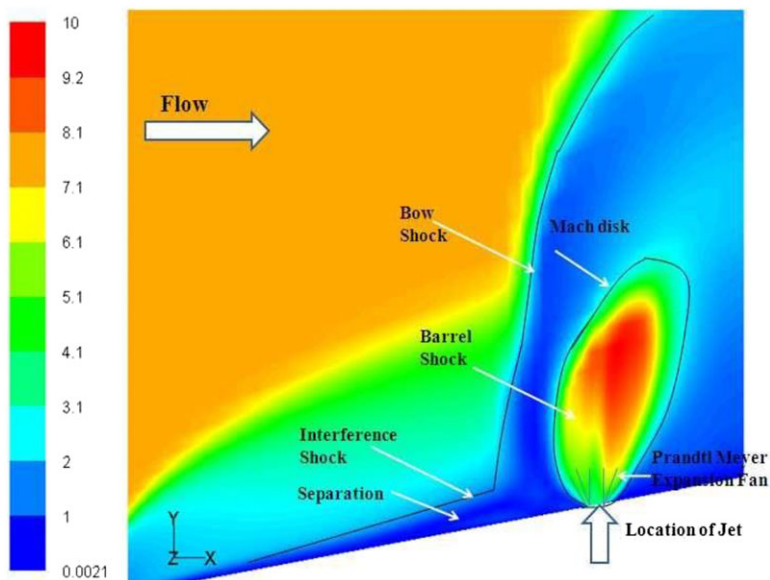


Figure 11. Sonic jet interactions with 8.1 Mach number external flow Mach contours at $\alpha = 5^\circ$.

stagnation region formed ahead of the jet and changes the flow field around the jet. This complex flow field changes the pressure variation along the leeward surface of the re-entry body. The stream lines near the jet interaction region are shown in Fig. 13 and the velocity vectors are shown in Fig. 14.

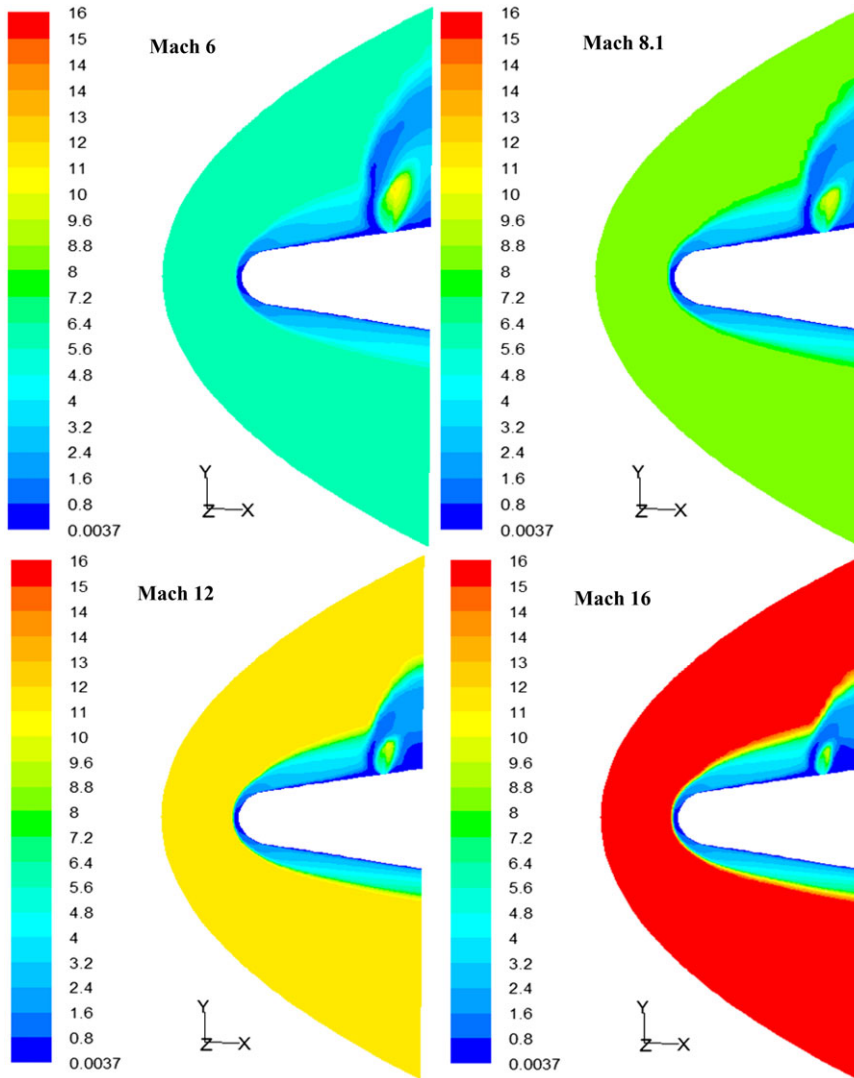


Figure 12. Mach contours at $M_\infty = 6, 8.1, 12$ and 16 at $\alpha = 5^\circ$, jet mass flow of 0.068kg/s .

5.4.2 Effect of Mach number on pressure distribution due to jet interaction

The pressure variation has been plotted in front of and behind the jet along the longitudinal direction at $\alpha = 5^\circ$ as shown in Fig. 15. All the upstream pressure distributions show a maximum pressure ahead of the jet and then decreased behind the jet. The magnitude of the maximum pressure increased with the Mach number and shifts towards the jet. This result is consistent with Dickman and Lu [30]. The induced jet interaction force also increased with the Mach number. The jet interaction force and the jet thrust are in the same direction. Hence the jet thrust is augmented strongly at high Mach numbers. Similarly the pitching moment produced by jet also augmented by moment produced by jet interaction force.

5.4.3 Influence of flight speed on aerodynamic characteristics due to jet interaction

The variation of flight performance and stability parameters at different Mach number for jet-off and jet-on conditions has been plotted in Fig. 16 at different Mach number. In jet-off condition, only external flow over the reentry vehicle was considered and the lateral jet is turned off. The normal force coefficient

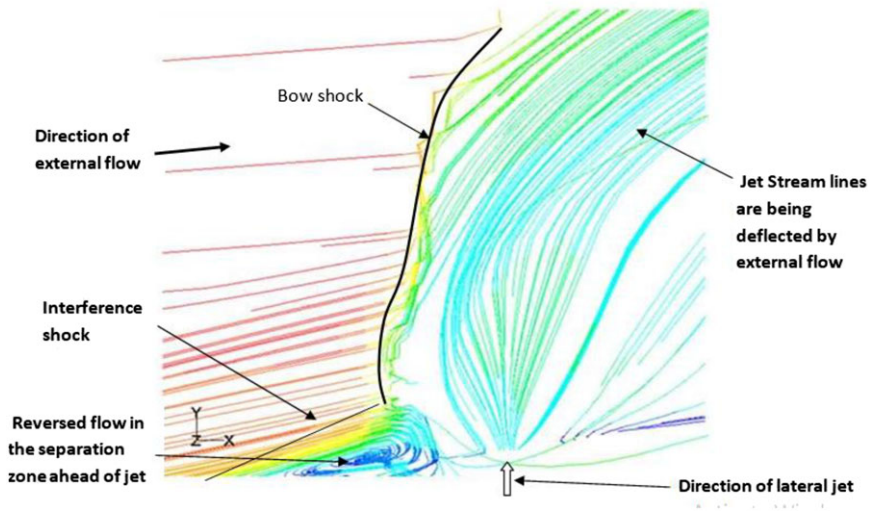


Figure 13. Zoomed view of streamlines in the jet interaction region.

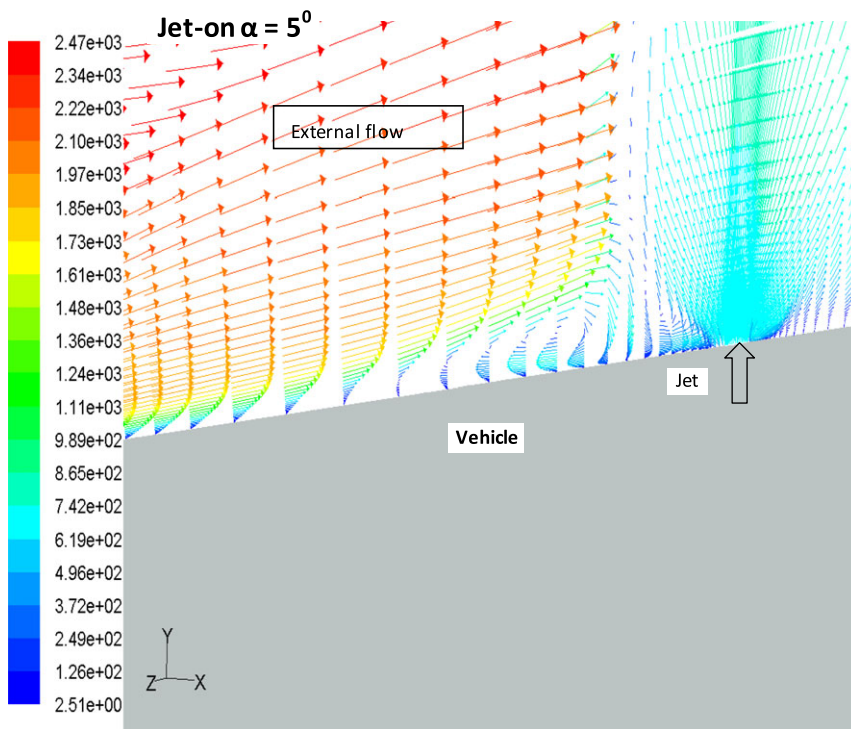


Figure 14. Velocity vectors in the jet interaction region.

decreased by 45.6% due to the jet on condition at Mach number 8.1. In case of Mach number 16, the reduction in normal force coefficient is 25.9%. The percentage of reduction is less at high Mach numbers compared with low Mach numbers. The pitching moment coefficient increased with the increase in Mach number for both jet-off and jet-on conditions. At Mach number 8.1, the reduction in C_m is with jet-on condition compared with jet-off is 48%, whereas at Mach number 16, the reduction in C_m as 29.6%.

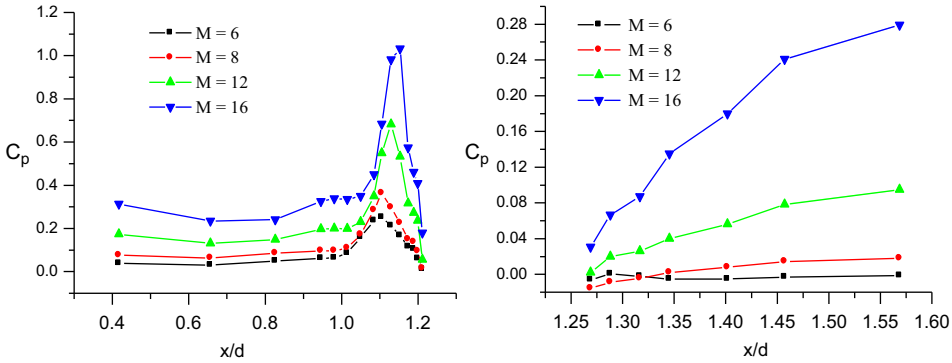


Figure 15. Upstream and downstream pressure distribution for jet-on condition at $M_\infty = 6, 8.1, 12$ and 16 .

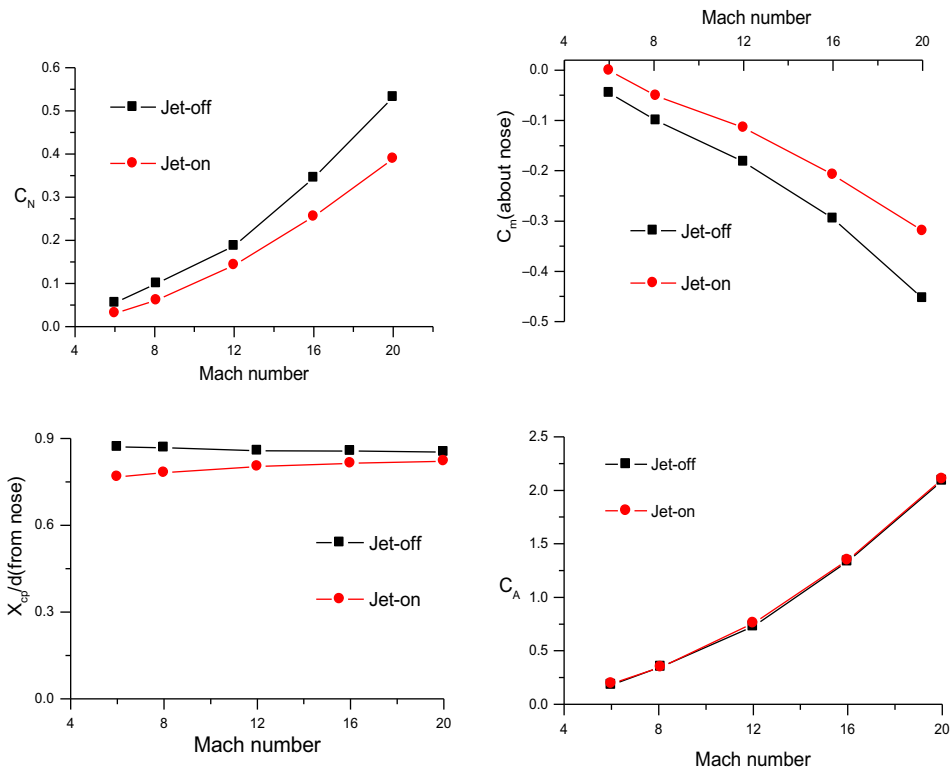


Figure 16. Variation of C_N , C_m , centre of pressure and C_A with Mach number.

The percentage of reduction is less at higher Mach numbers compared with lower Mach numbers. For jet-off condition, the centre of pressure is not varying significantly with Mach number. The magnitude of the X_{cp}/d for jet-on condition is lower than the jet-off condition at the flight speeds considered in the simulations. This indicates that the centre of pressure shifts towards nose. The shift of the centre of pressure towards the base indicates an improvement in the stability of the vehicle. It was observed that the stability of the vehicle decreased with the jet-on condition compared with jet-off condition. This observation is consistent with the conclusion given by Ref. (31). The magnitude of the X_{cp}/d for jet-on condition is increased with the flight speed. The centre of pressure is shifting towards the base of the

vehicle as the flight speed increases. This indicates that the stability of the vehicle improves with the increase in flight speed. The axial force coefficient significantly increases with increase of Mach number of jet-on and jet-off conditions. The axial force coefficient is slightly higher with jet-on condition than the jet-off condition.

6.0 Conclusion

The performance and stability of the re-entry vehicle at different Mach numbers have been investigated when the jet is issued into the cross flow. The simulation results are summarised as follows.

1. The normal force coefficient is reduced by 45.6%, and the pitching moment coefficient is reduced by 48% due to the lateral jet interaction with the external flow. The centre of pressure shifts forward due to jet interaction by 0.06d at 8.1 Mach number and an angle-of-attack of 5° . This indicates that the aerodynamic stability of the vehicle is reduced due to the lateral jet interaction. Even a small jet of 2mm can produce significant aerodynamic forces on a hypersonic re-entry body, which can be applied to control the vehicle's orientation.
2. The lateral jet introduced into the external flow alters the surface pressure distribution, and significant modifications in the flow field were observed near the jet. Over pressure in the upstream region of the jet and under pressure in the wake region create the pitching moment on re-entry vehicle.
3. Computational results indicate a strong jet interaction with the external flow at higher Mach numbers.
4. The stability of the vehicle has been studied at various Mach numbers. For the jet-on condition, the centre of pressure shifts towards the base of the vehicle with an increase in Mach number. This indicates that the vehicle's stability improves with increasing flight speed.
5. The results of the study provide a better understanding of the interaction between the jet and cross flow on re-entry vehicle performance.

Competing interests. No potential Competing interests was reported by the author(s).

References

- [1] Kurita, M., Inoue, T. and Nakamura, Y. Aerodynamic interaction due to side jet from a blunted cone in hypersonic flow, Presented at the 18th Applied Aerodynamics Conference, Denver, CO, USA, August 14-17, 2000. <https://doi.org/10.2514/6.2000-4518>
- [2] Kurita, M., Okada, T. and Nakamura, Y. The effects of attack angle on aerodynamic interaction due to side jet from a blunted body in a supersonic flow. Presented at the 39th Aerospace Sciences Meeting and Exhibit, Reno, NV, USA, January 8-11, 2001. <https://doi.org/10.2514/6.2001-261>
- [3] Kurita, M., Okada, T. and Nakamura, Y. The effects of attack angle on side jet aerodynamic interaction in blunted body at hypersonic flow. Presented at the 10th AIAA/NAL-NASDA-ISAS International Space Planes and Hypersonic Systems and Technologies Conference, Kyoto, Japan, April 24-27, 2001. <https://doi.org/10.2514/6.2001-1825>
- [4] Kennedy, K., Walker, B. and Mikkelsen, C. Jet interaction effects on a missile with aerodynamic control surfaces, Presented at the 37th Aerospace Sciences Meeting and Exhibit, Reno, NV, USA, January 11-14, 1999. <https://doi.org/10.2514/6.1999-807>
- [5] Gnemmi, P. and Seiler, F. Interaction of a lateral jet with the projectile external flow, Atmospheric Flight Mechanics Conference, Denver, CO, USA, August 14-17, 2000. <https://doi.org/10.2514/6.2000-4196>
- [6] Erdem, E. and Kontis, K. Experimental investigation of sonic transverse jets in Mach 5 cross flow, *Aerosp. Sci. Technol.*, 2021, **110**, p 106419. <https://doi.org/10.1016/j.ast.2020.106419>
- [7] Srivastava, B. Computational analysis and validation for lateral jet controlled missiles, *J. Spacecr. Rockets*, 1997, **34**, (5), pp 584–592. <https://doi.org/10.2514/2.3272>
- [8] Hsieh, T. Computation and analysis of cross jet interaction flow fields of a bi-conic body at incidences, Presented at the 16th AIAA Applied Aerodynamics Conference, Albuquerque, NM, USA, June 15-18, 1998. <https://doi.org/10.2514/6.1998-2625>
- [9] Gimelshein, S.F., Alexeenko, A.A. and Levin, D.A. Modeling of the interaction of a side jet with a rarefied atmosphere, *J. Spacecr. Rockets*, 2002, **39**, (2), pp 168–176. <https://doi.org/10.2514/2.3814>

- [10] Nakamura, T., Kaneko, M., Menshov, I. and Nakamura, Y. Numerical simulation on aerodynamic interaction between a side jet and flow around a blunt body in hypersonic flow, Presented at the 41st Aerospace Sciences Meeting and Exhibit, Reno, Nevada, January 6-9, 2003. <https://doi.org/10.2514/6.2003-1135>
- [11] Valerio, V., Joseph, S. and Reece, N. Comparison of first and second Order turbulence models for a Jet/3D ramp combination in supersonic flow, Presented at the 43rd AIAA Aerospace Sciences Meeting and Exhibit, Reno, Nevada, January 10-13, 2005. <https://doi.org/10.2514/6.2005-1100>
- [12] Gnemmi, P. and Hans, J.S. Experimental and numerical investigations of a transverse jet interaction on a missile body, Presented at the 43rd AIAA Aerospace Sciences Meeting and Exhibit, Reno, Nevada, January 10-13, 2005. <https://doi.org/10.2514/6.2005-52>
- [13] Gnemmi, P., Adeli, R. and Longo, J. Computational comparisons of the interaction of a lateral jet on a supersonic generic missile, Presented at the AIAA Atmospheric Flight Mechanics Conference and Exhibit, Honolulu, Hawaii, August 18-21, 2008. <https://doi.org/10.2514/6.2008-6883>
- [14] Gnanaskandan, A. and Chakraborty, D. Numerical simulation of transverse side jet interaction with supersonic free stream, *Aerosp. Sci. Technol.*, 2010, **14**, (5), pp 295–301. doi: [10.1016/j.ast.2010.02.001](https://doi.org/10.1016/j.ast.2010.02.001)
- [15] Rasheed, I. and Mishra, D.P. Numerical study of a sonic jet in a supersonic cross flow over a flat plate, *Phys. Fluids*, 2020, **32**, p 126113. <https://doi.org/10.1063/5.0026214>
- [16] Yadav, K.R., Paul, A.R., Hegde, N. and Jain, A. A comparison of circular and slotted synthetic jets for flow control in a twin air-intake, *Def. Sci. J.*, 2020, **70**, (2), pp 113–121. <https://doi.org/10.14429/dsj.70.13053>
- [17] Kislovskiy, V.A. and Zvegintsev, V.I. Investigation of flight dynamics of an axisymmetric vehicle with ejection of a lateral transverse jet, *Thermophys. Aeromech.*, 2020, **27**, pp 61–69. <https://doi.org/10.1134/S0869864320010059>
- [18] Choi, K., Lee, S., Oh, K. and Kim, C. Numerical investigation of jet interactions for a lateral thrust jet controlled interceptor operating at medium altitudes, *Int. J. Aeronaut. Space Sci.*, 2020, **21**, pp 39–49. <https://doi.org/10.1007/s42405-019-00209-x>
- [19] Bhagat, A., Gijare, H. and Dongari, N. Modeling of a reaction control jet interacting with high-speed cross-flow in slip flow regime, *Proc. Inst. Mech. Eng. Part G*, 2019, pp 1–16. doi: [10.1177/0954410019836901](https://doi.org/10.1177/0954410019836901)
- [20] Kang, K.T. and Lee, S. Modeling and assessment of jet interaction database for continuous-type side jet, *J. Spacecr. Rockets*, 2017, **54**, (4), pp 1–14. doi: [10.2514/1.A33807](https://doi.org/10.2514/1.A33807)
- [21] Miller, W.A., Medwell, P.R., Doolan, C.J. and Kim, M. Transient interactions between a reaction control jet and hypersonic cross flow, *Phys. Fluids*, 2018, **30**, p 046102. doi: [10.1063/1.5018877](https://doi.org/10.1063/1.5018877)
- [22] Chen, J., Liu, Y. and Bo, J. Numerical simulation of lateral jet interaction, *J. Appl. Math. Phys.*, 2017, **5**, (9), pp 1686–1693. doi: [10.4236/jamp.2017.59141](https://doi.org/10.4236/jamp.2017.59141)
- [23] Zhang, J., Lei, J., Yin, J. and Niu, J. The numerical investigation on the rolling decoupling of a canard-controlled missile using the jet control system, *Eng. Appl. Comput. Fluid Mech.*, 2020, **14**, (1), pp 1062–1077. doi: [10.1080/19942060.2020.1799866](https://doi.org/10.1080/19942060.2020.1799866)
- [24] Dong, H., Liu, J., Chen, Z. and Zhang, F. Numerical investigation of lateral jet with supersonic reacting flow, *J. Spacecr. Rockets*, 2018, **55**, pp 928–935. doi: [10.2514/1.A34096](https://doi.org/10.2514/1.A34096)
- [25] Dong, M., Liao, J., Du, Z. and Huang, W. Influences of lateral jet location and its number on the drag reduction of a blunted body in supersonic flows, *J. Aeronaut. Sci.*, 2020, pp 1–15. doi: [10.1017/aer.2020.4](https://doi.org/10.1017/aer.2020.4)
- [26] Zhao, M., Bian, Y., Li, Q. and Ye, T. Large eddy simulation of transverse single/double jet in supersonic cross flow, *Aerosp. Sci. Technol.*, 2019, **89**, pp 31–45. <https://doi.org/10.1016/j.ast.2019.03.044>
- [27] Grandh, R.K. and Roy, A. Performance of control jets on curved bodies in supersonic cross flows, *J. Spacecr. Rockets*, 2019, pp 1–12. <https://doi.org/10.2514/1.A34314>
- [28] Li, J., Chen, S., Cai, F., Wang, S. and Yan, C. Bayesian uncertainty analysis of SA turbulence model for supersonic jet interaction simulations, *Chin. J. Aeronaut.*, 2022, **35**, (4), pp 185–201. <https://doi.org/10.1016/j.cja.2021.07.039>
- [29] Dharavath, M., Manna, P. and Chakraborty, D. Computational study of transverse slot injection in supersonic flow, *Def. Sci. J.*, 2018, **68**, (2), pp 121–128. doi: [10.14429/dsj.68.11069](https://doi.org/10.14429/dsj.68.11069)
- [30] Dickmann, D.A. and Lu, F.K. Jet in supersonic cross flow on a flat plate, Presented at the 25th AIAA Aerodynamic Measurement Technology and Ground Testing Conference, San Francisco, California, June 5-8, 2006. <https://doi.org/10.2514/6.2006-3451>
- [31] Zhang, L., Yang, J., Duan, T., Wang, J., Li, X. and Zhang, K. Numerical and experimental investigation on nosebleed air jet control for hypersonic vehicle, *J. Aerosp.*, 2023, **10**, (552) pp 1–23. <https://doi.org/10.3390/aerospace10060552>